

SENSITIVITY OF MICROPHYSICAL PARAMETERS ON THE EVOLUTION OF A SUPERCELL

Samuel P. Lillo^{1,2}, Edward R. Mansell³

¹ National Weather Center Research Experiences for Undergraduates Program
and

² Plymouth State University
Plymouth, NH

³ NOAA/National Severe Storms Laboratory
University of Oklahoma, Norman, Oklahoma

ABSTRACT

Due to limited computational resources, critical microphysical processes must be accounted for in models through parameterization schemes. These schemes use many constants that have large uncertainties and may vary in nature spatially and temporally. By perturbing individual parameters within a single scheme, an ensemble can be created to attempt to account for the uncertainty in the model physics.

Five ensembles are created to test the sensitivity of a simulated supercell to the following parameters: cloud condensation nuclei (CCN) concentration, the efficiency of cloud water collection by graupel and hail, the fraction of liquid water allowed on graupel and hail, rime density function, and the drag coefficient as a function of particle density. A range of values was chosen for each parameter to represent the uncertainty that exists within the model microphysics. All ensembles exhibited growing variance through the simulation. Monotonic association to the storm evolution was most prominent in the CCN ensemble, in which there were notable variance in the track and intensity of the supercell.

1. INTRODUCTION

In atmospheric modeling, errors and biases in the initial conditions and model physics result in an uncertainty in the forecast. This will always be a detriment to deterministic prediction. Model ensembles have become a popular method of dealing with the uncertainty, in which initial conditions and model physics are perturbed in each member. Ensembles have been used successfully for some time in synoptic scale forecasting, however an interest in storm scale ensembles has grown considerably. For example, the NSSL Warn-On-Forecast project has proposed the use of ensembles for developing probabilistic severe weather forecasts and advanced warnings (Stensrud et al., 2009).

One significant limitation in storm scale modeling is the need for microphysical

parameterizations to account for the numerous possible hydrometeor modes, their characteristics, and their interactions with each other.

Computational resources limit the extent to which these parameterizations can accurately represent microscale processes in the cloud.

Stensrud et al. (2000) used two model ensembles, one perturbing initial conditions, and the other varying model physics, to test their usefulness in forecasting a mesoscale convective complex. They found that the forecasts produced by the model physics ensemble exhibited a much faster growing variance than the initial conditions ensemble. This suggests that addressing model physics uncertainty is a key component in creating a more useful ensemble.

Stensrud employed different convective and boundary layer parameterization schemes to develop the ensemble. However, Gilmore et al. (2004) demonstrated that perturbing individual parameters within a single scheme can produce effective variation in the forecast as well. Gilmore varied the intercept parameters for the distribution

¹ Corresponding author address: Samuel P. Lillo
592 Hurricane Rd. Keene, NH 03431
splillo@plymouth.edu

of graupel sizes in a single moment scheme, and found notable differences between ensemble members in the evolution of the storm. This provided motivation to look at the effect of other parameters within a more sophisticated scheme.

2. METHODOLOGY

This study uses the Collaborative Model for Multiscale Atmospheric Simulation (COMMAS) (Wicker and Wilhelmson, 1995). This model utilizes a multi-moment microphysical parameterization scheme which predicts the mass mixing ratio and number concentration of cloud droplets, cloud ice, rain drops, snow crystals, graupel, and hail. A third moment is the predicted radar reflectivity of graupel, hail, and rain (Mansell et al., 2010).

For the main part of this study, the model was initialized with a horizontally homogeneous environment based on an observed sounding near Hub, TX at 2058 UTC on June 2, 1995. This day featured an outbreak of long-lived supercells over the west Texas panhandle. Simulations were performed in a 100km by 100km by 20km domain with horizontal grid spacing of 1km, and a stretched vertical grid spacing ranging from 200m at the bottom of the domain up to a maximum of 500m at the top. Convection was initialized by a boundary layer updraft forcing term with a maximum vertical acceleration of $6.0 \times 10^{-2} \text{ m/s}^2$ at the center of the domain. Forcing was applied for the first 15 minutes of the simulation. The model was run out to three hours.

Five parameters were tested for forecast sensitivity: the concentration of cloud condensation nuclei (CCN), the efficiency of cloud water collection by graupel and hail (EHW), the maximum fraction of liquid water allowed on graupel and hail (FWMH), the drag coefficient as a function of hydrometeor density, and rime density function. These parameters and their ranges of values were chosen based on previous research, general experience, and curiosity. All of these ranges appropriately represent the envelope of uncertainty in atmospheric conditions and processes. The control run (CNTL) maintains all the default values of parameters in the model,

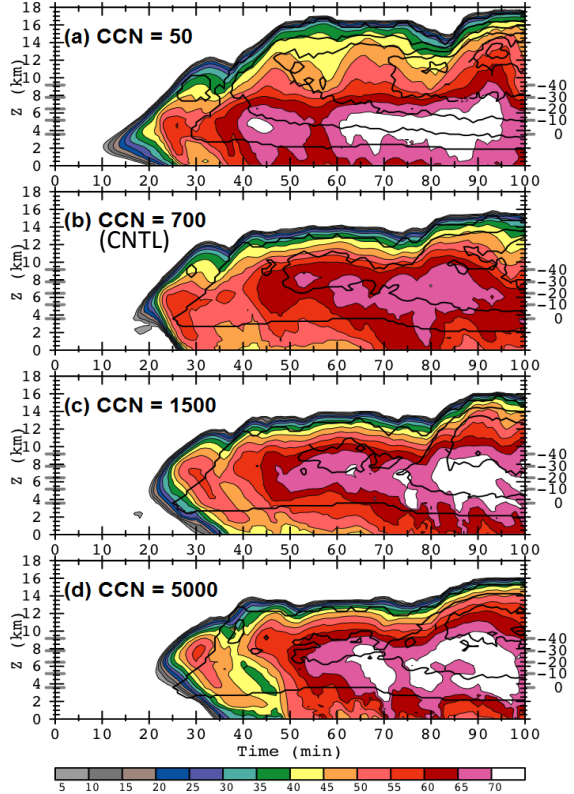


Figure 1: Time-height sections of maximum reflectivity (color fill) and updraft volume (black contours) for CCN concentrations of a) 50, b) 700 (CNTL), c) 1500, and d) 5000.

particularly CCN concentration of 700cm^{-3} , EHW of 1.0 (sec. 3.2), and FWMH of 0.5 (sec.3.3).

3. RESULTS

Results of each ensemble were based on primarily qualitative comparisons between each member. Variables used for comparison include patterns in radar reflectivity, the extent and intensity of the low level cold pool, maximum updraft velocity and volume, and the total mass and density of rain, graupel, and hail.

3.1 Concentration of CCN

The effects of CCN concentration in the parent airmass on cloud microphysics is well acknowledged. These effects impact precipitation processes that are important in forecasting storm evolution and sensible weather at the surface. However, CCN concentration is not a regularly measured variable despite the fact that it can

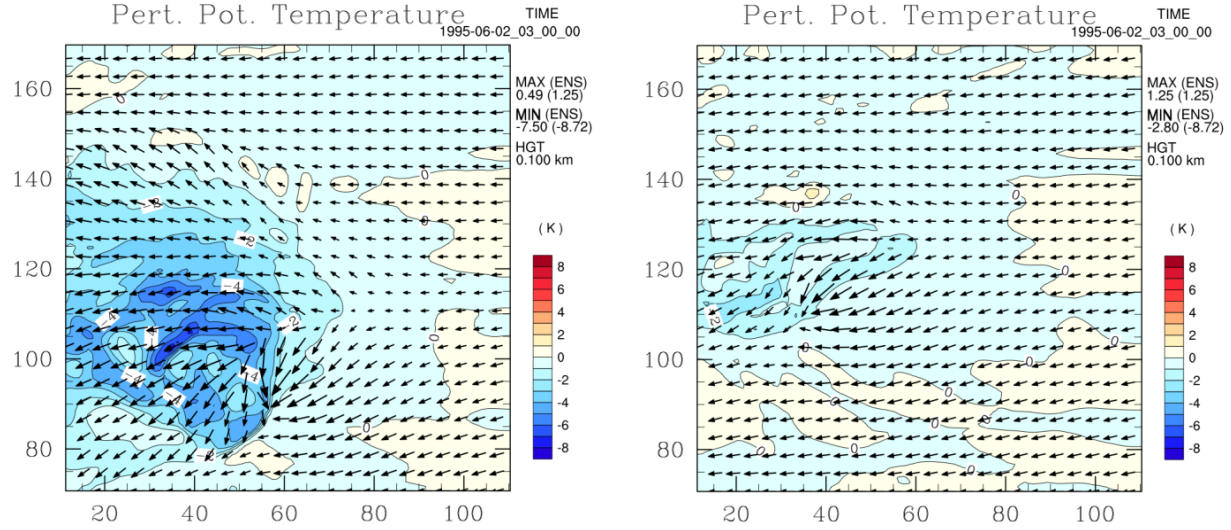


Figure 2: Perturbation potential temperature and storm relative wind vectors at 100m height at 3 hours into the model run for (left) CCN = 200cm⁻³ and (right) CCN = 2500cm⁻³.

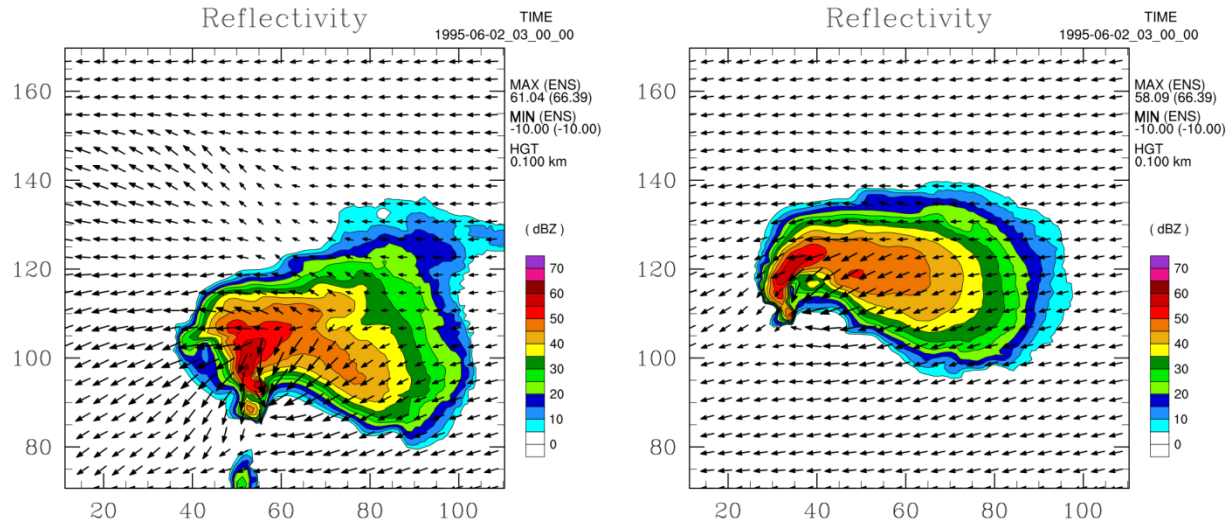


Figure 3: Radar reflectivity and storm relative wind vectors at 100m height at 3 hours into the model run for (left) CCN = 200cm⁻³ and (right) CCN = 2500cm⁻³.

range considerably between different airmasses. Without observations, its value must be assumed in the initial conditions of the model.

Nine members were run with the following CCN concentrations: 1) 50cm⁻³, 2) 200cm⁻³, 3) 350cm⁻³, 4) 500cm⁻³, 5) 700cm⁻³, 6) 1000cm⁻³, 7) 1500cm⁻³, 8) 2500cm⁻³, and 9) 5000cm⁻³. The control run is member 5 with a concentration of 700cm⁻³. The lower CCN cases exhibited faster growth of intial rain drops due to accelerated warm

rain processes. High CCN cases featured minimal warm rain generation due to higher concentrations of smaller drops which decreases the rate of coalescence. As a result, initial precipitation reached the ground ten to fifteen minutes later than the lower CCN cases (Fig. 1).

These initial differences have ramifications on the rest of the storm evolution. The faster onset of precipitation in the low CCN members results in the low level cold pool developing earlier and

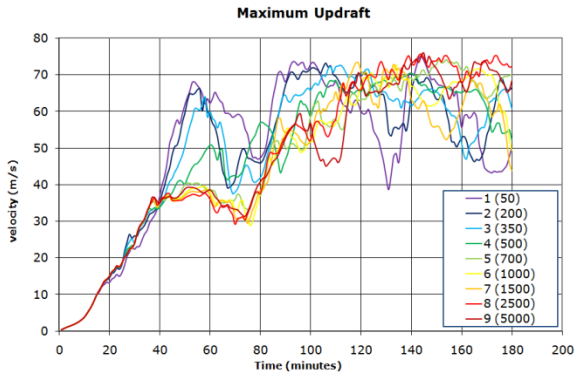


Figure 4: Maximum updraft velocity in the domain, over time, for each member of the CCN ensemble.

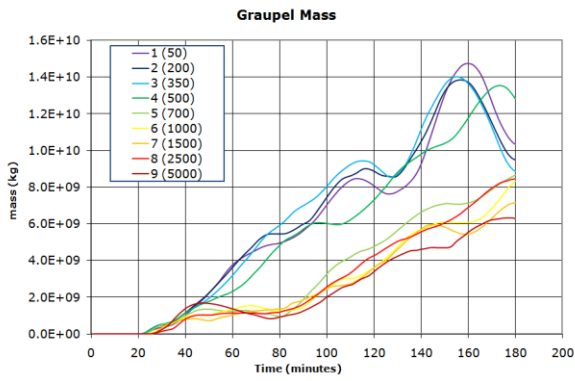


Figure 5: Total graupel mass in the domain, over time, for each member of the CCN ensemble.

becoming stronger (Fig. 2). The enhanced upward forcing on the boundary of the cold pool builds the storm further to the right of the mean environmental wind. Over time, the storms that were initiated in a lower CCN airmass track significantly further right than the higher CCN cases (Fig. 3).

Another interesting result was a distinct difference in the evolution of the updraft intensity. All cases exhibited a steadily intensifying updraft through the first 40 minutes of the simulation (Fig. 4), however beyond that time, the cases diverge. Higher CCN cases level off, while low CCN cases continue to intensify due to higher CAPE air near the surface being forced to rise on the boundary of the cold pool. As a result, the low cases feature a greater updraft velocity (Fig. 4), updraft volume, and higher echo tops (Fig. 1) than the high cases at 50 to 60 minutes. This bifurcation is also noticeable in the total graupel mass, and is

maintained through the entire simulation (Fig. 5). The divergence in the updraft intensity is notable through 80 minutes before nonlinear growth of perturbations in the storm evolution becomes more prevalent.

The low CCN cases appear to undergo periodic oscillations in intensity while the high CCN cases show a more steady linear growth (Fig. 1 and 4). By the end of the run, little apparent association remains between intensity and CCN, though the patterns of oscillation versus linear growth continue.

3.2 Efficiency of cloud water collection by graupel and hail

Within the model, the efficiency of the collection of cloud water by graupel and hail is held as a constant parameter (EHW) that may range from 0 to 1.0. Seven members were run with the following prescribed EHW: 1) 1.0, 2) 0.9, 3) 0.8, 4) 0.7, 5) 0.6, 6) 0.5, and 7) 0.4. The control run is member 1 with an EHW of 1.0.

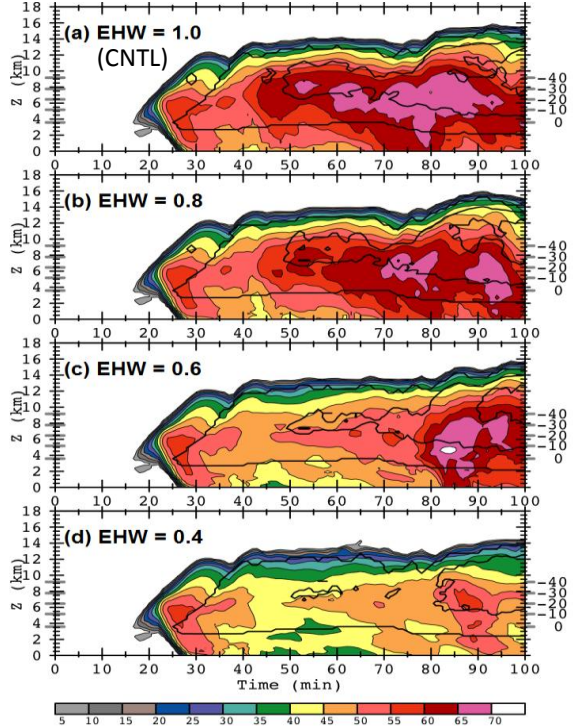


Figure 6: Time-height sections of maximum reflectivity (color fill) and updraft volume (black contours) for efficiency of a) 1.0 (CNTL), b) 0.8, c) 0.6, and d) 0.4.

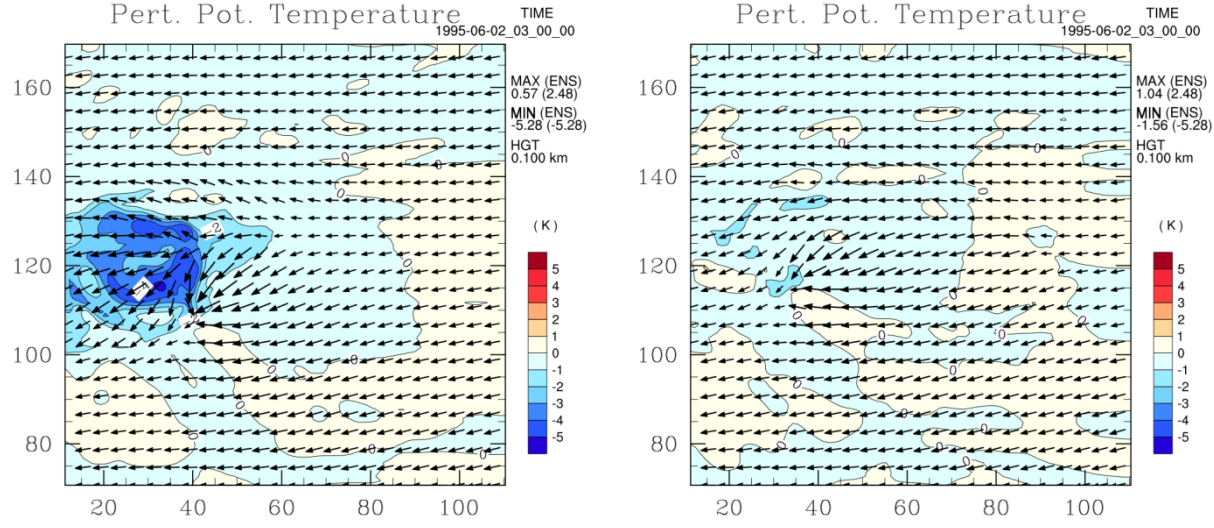


Figure 7: Perturbation potential temperature and storm relative wind vectors at 100m height at 3 hours into the model run for (left) EHW = 1.0 and (right) EHW = 0.5.

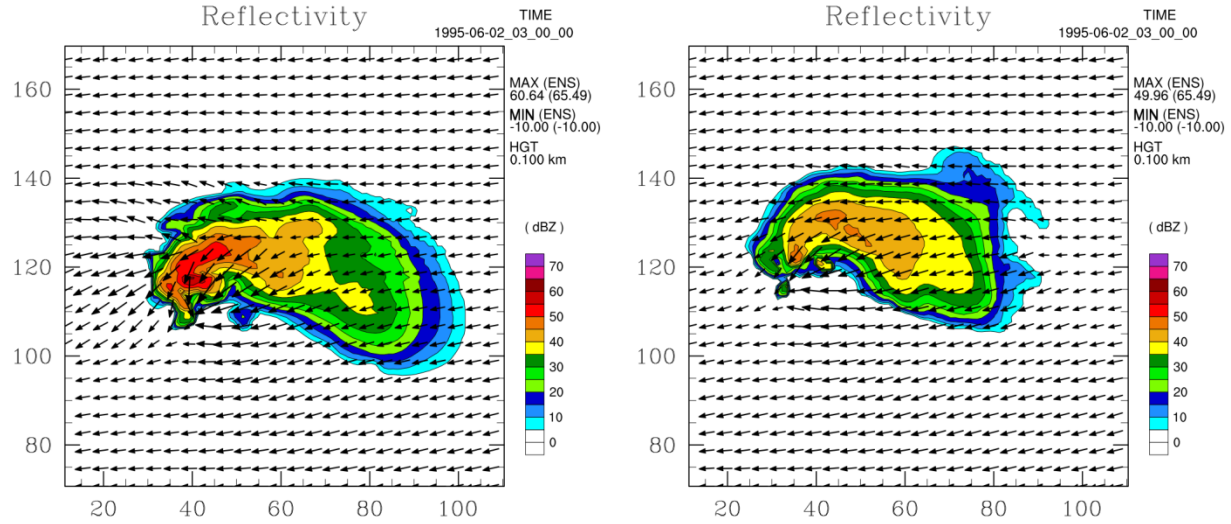


Figure 8: Radar reflectivity and storm relative wind vectors at 100m height at 3 hours into the model run for (left) EHW = 1.0 and (right) EHW = 0.5.

There is little spread in the first 30 minutes of development. Beyond 30 minutes, the members with higher collection efficiency developed much higher radar reflectivity than the low cases which in fact experience decreasing reflectivity (Fig. 6). Less cloud droplet and cloud ice mass is observed in the higher efficiency cases since more of the cloud water is being accreted onto graupel. The growth of graupel is more heavily influenced by collection efficiency when there is larger graupel

doing the collecting. The variation in efficiency thus does not impact the initial development of reflectivity but has significant ramifications later in the simulation.

Precipitation fallout is reduced significantly in the lower efficiency cases, since the main source for rain is graupel and hail melt. As a result, the low level cold pool is drastically weaker in the low efficiency cases than the higher cases (Fig. 7). Similar to the CCN ensemble, differences

in the track of the storm arise as a result of forcing along the boundary of the cold pool. The higher efficiency cases track slightly to the right of the lower cases (Fig. 8). In addition, the stronger cold pool in the high cases yields stronger forcing on the boundary that enhances the updraft (Fig. 6). There is less spread in the updraft velocity as in the CCN ensemble, but it maintains a monotonic association to the EHW throughout the simulation.

3.3 Maximum fraction of liquid water allowed on graupel and hail

Within the model, the maximum fraction of liquid water that is allowed to be carried on graupel and hail is held as a constant parameter (FWMH) that may range from 0 to 1.0 (Ferrier, 1994). Nine members were run with the following

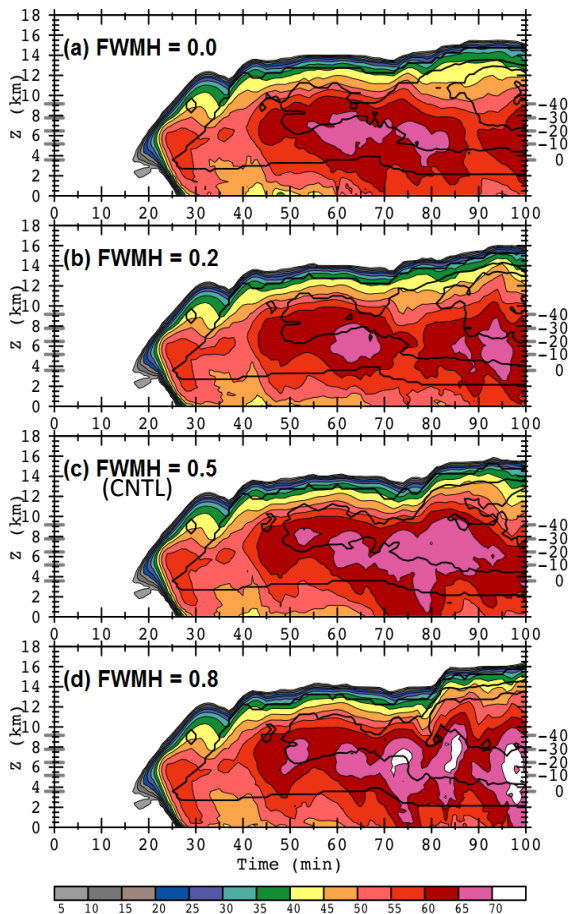


Figure 9: Time-height sections of maximum reflectivity (color fill) and updraft volume (black contours) for FWMH of a) 0.0, b) 0.2, c) 0.5 (CNTL), and d) 0.8.

prescribed maximum fractions: 1) 0.0, 2) 0.1, 3) 0.2, 4) 0.3, 5) 0.4, 6) 0.5, 7) 0.6, 8) 0.7, 9) 0.8. The control run is member 6 with a FWMH of 0.5.

Each member evolves very similarly through the first 60 minutes of the simulation. Beyond 60 minutes, differences from nonlinear growth amplify, but no monotonic association is discernable. Horizontal slices of radar reflectivity at 100m show few differences even through the end of the run. Higher FWMH does tend to result in higher reflectivity (Fig. 9) in the core of the storm due to larger particles being recycled into the updraft and possibly addition from wet growth of hail. Large variation, particularly in hail mass, develops after 70 minutes. However, graupel, hail, and rain total mass show little systematic association to FWMH.

3.4 Rime density function

Macklin (1962) determined that the density of ice accreted on graupel and hail is a function of the median cloud droplet volume radius r (μm), impact velocity V_0 (m/s), and the temperature of the riming surface T_s ($^{\circ}\text{C}$). Specifically, Macklin developed the parameter rV_0/T_s , with a general equation form of

$$\rho_{\text{rime}} = \text{rimc1} \times (rV_0/T_s)^{\text{rimc2}} \quad (1)$$

where ρ_{rime} is the density of rime in kg m^{-3} , and rimc1 and rimc2 are constants. Macklin determined empirically a value for rimc1 of 110, and rimc2 of 0.76. The function is capped below the density of ice, near 900 kg m^{-3} . Pflaum and Pruppacher (1979), from their own empirical evaluation, found values of 261 and 0.38 respectively. The default in COMMAS is 300 and 0.44 (Rasmussen and Heymsfield, 1985). These three equations are shown plotted in figure 10.

In order to test the sensitivity to the rime density function, an ensemble was created with the density increasing monotonically by member. Six members were created using the same general formula, and varying values of rimc1 and rimc2 (see Table 1). The ensemble encompasses the solutions from Macklin, Pflaum, and the default. The six members are shown plotted in figure 11. The control run is member 4.

	1	2	3	4	5	6
Rimc1	100	150	200	250	300	350
Rimc2	0.65	0.6	0.55	0.525	0.5	0.475

Table 1: Rimc1 and rimc2 values for each rime density function ensemble member.

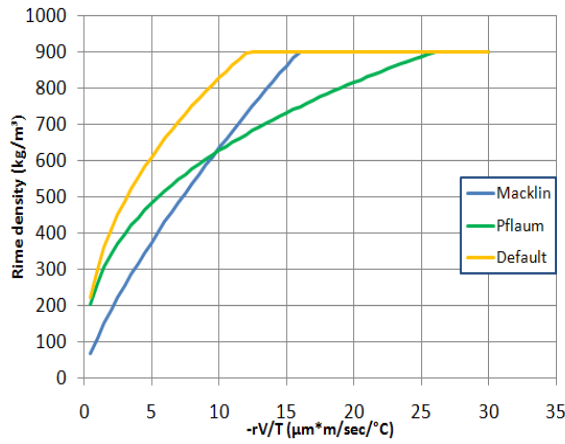


Figure 10: Rime density as a function of the parameter $-rV_0/T_s$, from Macklin (1962), Pflaum and Pruppacher (1979), and the COMMAS default.

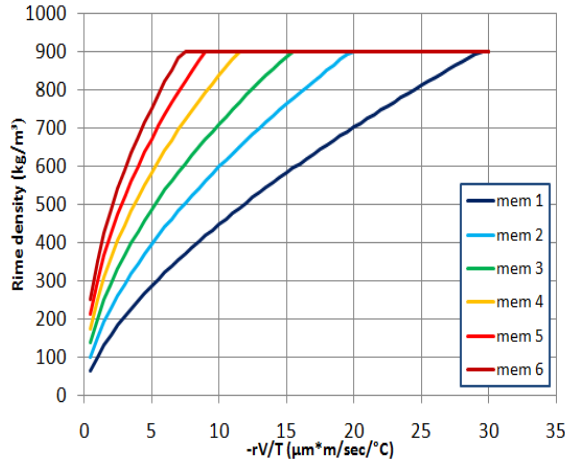


Figure 11: Rime density as a function of the parameter $-rV_0/T_s$ for the six members of the ensemble.

Each member evolves similarly through the first 40 minutes. Beyond 40 minutes, larger graupel develops in the lower density members. Given the same mass of cloud drops in the cloud,

lower density ice accretion would result in greater volume. Larger, low density graupel will have a greater drag coefficient and thus be suspended in the cloud, during which time it grows. This process accelerates the spread between members. Also as a result, higher radar reflectivity appears in the lower density members (Fig. 12), and continues through the simulation.

The lower density members develop higher graupel mass in the first 50 minutes due to the process described above. By this time, graupel conversion to hail is increasing. Members diverge

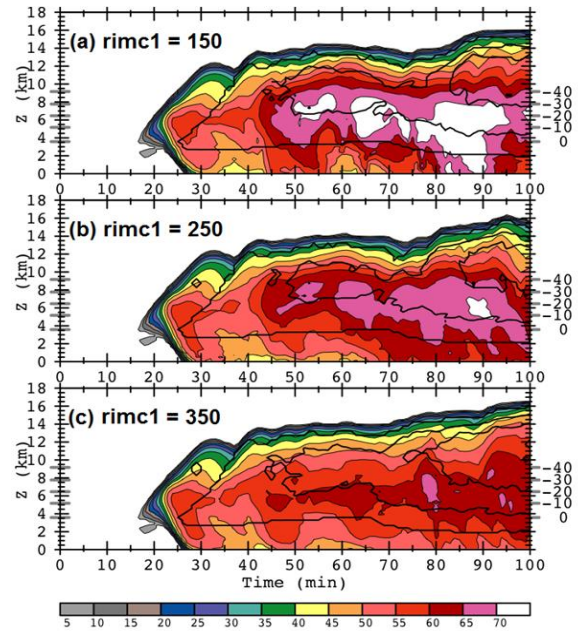


Figure 12: Time-height sections of maximum reflectivity (color fill) and updraft volume (black contours) for rime density members a) 2, b) 4, and c) 6.

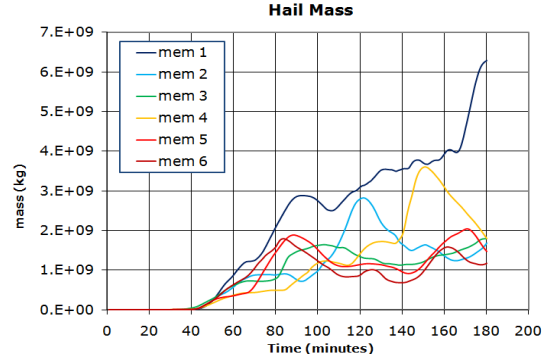


Figure 13: Total mass of hail in the domain, over time, for each member of the rime density ensemble.

quickly beyond 50 minutes. The lowest density member (1) appears as a clear outlier, with periods of rapid hail production that generates around five times the mass of the other members by the end of the simulation (Fig. 13). An experimental run with $\text{rimc1} = 50$ (not shown) yielded similar results to member 1 ($\text{rimc1} = 100$).

3.5 Drag coefficient

The terminal velocity of graupel is related to the drag coefficient by the following equation (Wisner, 1972):

$$V_T = \gamma \left(\frac{4\rho_g g}{3C_D \rho_{air}} \right)^{\frac{1}{2}} D^{\frac{1}{2}} \quad (2)$$

where γ is the fall speed factor, ρ_g is the density of graupel, g is the acceleration due to gravity, ρ_{air} is the density of air, D is the diameter of the graupel, and C_D is the drag coefficient (Mansell 2010). The terminal fall speed is thus proportional to the inverse of the square root of the drag coefficient.

In the model, the drag coefficient is defined as a linear function of particle density. The coefficient is a maximum (cdhmax) at low densities, followed by a linear decrease between the low density (cdhdmin) and high density (cdhdmax), ending at a minimum value (cdhmin) through high densities. The default parameter values are $\text{cdhmin} = 0.45$, $\text{cdhmax} = 1.0$, $\text{cdhdmin} = 500$, and $\text{cdhdmax} = 800$. An initial ensemble was created by varying all of the parameters together to produce a representative distribution. The best spread was found with

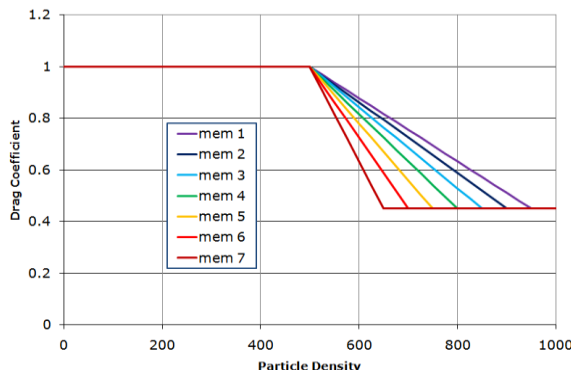


Figure 14: Drag coefficient as a function of particle density for the seven members of the ensemble.

varying cdhdmax . Based on that result, a seven member ensemble was created with the following cdhdmax : 1) 950, 2) 900, 3) 850, 4) 800, 5) 750, 6) 700, 7) 650. The control is member 4. The seven members are shown plotted in figure 14. Note that between cdhdmin and cdhdmax , the drag coefficient decreases by member, and thus the terminal velocity of graupel increases by member.

While this ensemble did yield notable variance, many of the measurands mentioned in the methods section showed little systematic association to the parameter. The most significant association was in the horizontal 100m radar reflectivity pattern. Lower cdhdmax (higher terminal velocity) resulted in a slight deviation in the track of the storm to the right of the lower velocity members. In addition, higher cdhdmax (lower terminal velocity) members featured a forward flank that extended further east (Fig. 15). This could be explained by the fact that with a lower fall speed, more time is available for hydrometeors to be transported downstream before reaching the ground.

4. CCN ENSEMBLE BY CAPE AND SHEAR

Of the five parameters tested, CCN concentration exhibited the greatest variance and monontonic trend in characteristics. The two most intriguing characteristics were also the most fundamental to forecasting: the track and intensity of the storm.

From the supercell case on June 2, 1995, the members with lower CCN concentration developed a stronger updraft, and tracked the storm significantly to the right of the higher CCN members. One viable explanation for both the track and intensity differences is the earlier development of the low level cold pool.

In a study by Mansell and Ziegler (2010), CCN concentration was varied in a similar range in examining effects on a small multicell storm. In time-height sections included in the paper, the updraft volume increases with increasing CCN, in contrast to the results of the current study. The small storm study was initiated with a notably lower CAPE and lower shear environment.

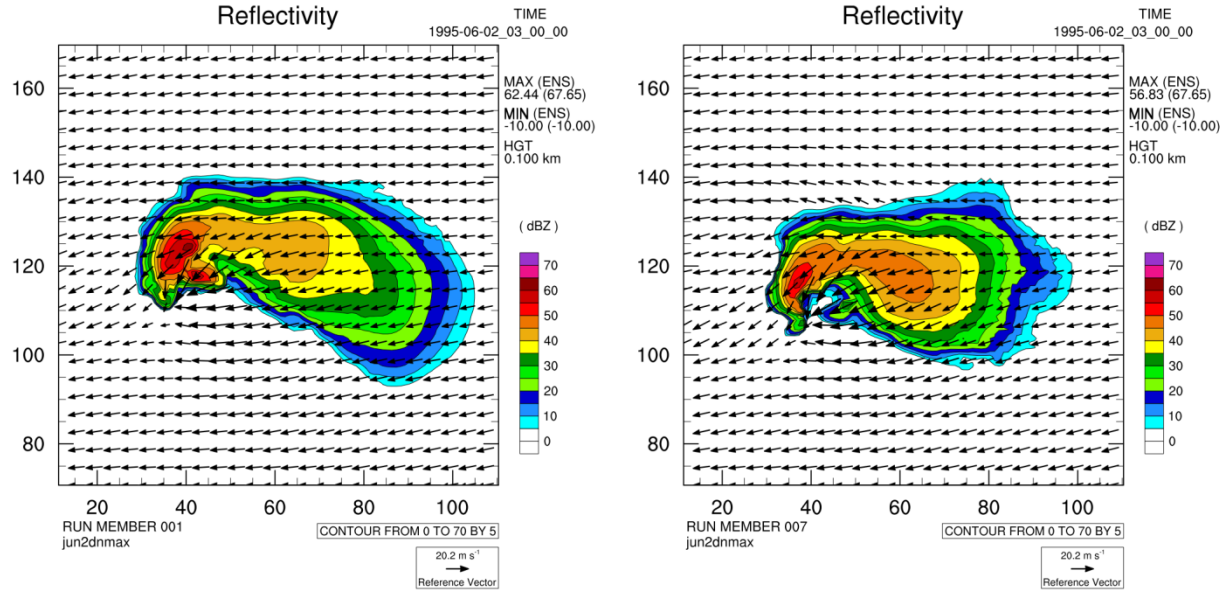


Figure 15: Radar reflectivity and storm relative wind vectors at 100m height at 3 hours into the model run for (left) $\text{cdhdnmax} = 950$ and (right) $\text{cdhdnmax} = 650$.

Based on these differences, another ensemble was created to test the influence of the initial environment in combination with CCN variation. using a thermodynamic profile from Weisman and Klemp (1982), and a half circle hodograph as described by Weisman and Klemp (1984). The members were split into low-CAPE and moderate-CAPE environments based on a surface mixing ratio of 12g/kg and 14g/kg, respectively. In those two groups, the members were further split into low-shear and high-shear environments based on a shear vector

magnitude of 20m/s and 50m/s, respectively. Finally, in the four resulting groups, there was one low CCN member with a concentration of 50cm^{-3} and one high CCN member with a concentration of 5000cm^{-3} , for a total of eight members.

The updraft velocity is plotted over time for each case in figure 16. In order to smooth stochastic variation, the plot is a 15 minute moving average. Steady development is observed for the first 30 minutes with no variation between CCN members. As to be expected, the high CAPE cases develop first, and the low shear cases develop the fastest. Between 30 and 50 minutes, all high CCN members level off while all low CCN members continue to develop, as observed in the current study. After 50 minutes, the high-CAPE/high-shear ensemble maintains the same relationship, while both low-shear ensembles flip, with the low CCN cases weakening considerably. This relationship continues through the rest of the simulation.

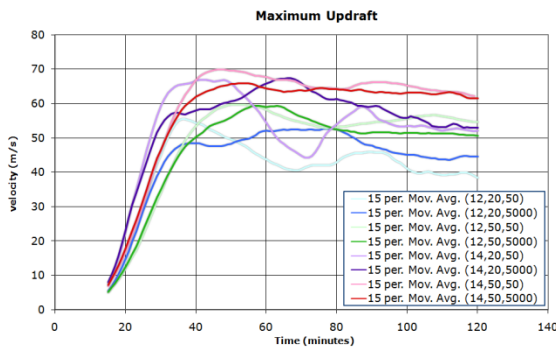


Figure 16: Maximum updraft velocity in the domain over time for each member of the CCN by CAPE and shear ensemble. The heavy shaded lines are high CCN members and the light shaded lines are low CCN members.

5. CONCLUSION

Several parameters within microphysics parameterization schemes are held constant or simplified due to computational limitations or insufficient observations for realistic conditions. As

a result, models cannot capture the true state of the atmosphere, and forecasts diverge from reality. The question is how much an individual parameter can affect the outcome of a forecast.

Five parameters were tested by running an ensemble incorporating a range of values. The five parameters were CCN concentration, the efficiency of cloud water collection by graupel and hail, the maximum fraction of liquid water allowed on graupel and hail, the drag coefficient as a function of hydrometeor density, and rime density.

All ensembles exhibited growing variance shortly after the development of the storm in the model. This indicates that for any one of these parameters, their value has ramifications on the forecast. Model variance appeared in a number of ways: linear monotonic association, bifurcation, outliers, and nonlinear growth of perturbations (which was featured in all ensembles). The clearest variance by association and bifurcation appeared with the CCN, EHW, and FWMH ensembles. The CCN ensemble in particular displayed a larger variance and association to storm evolution. For example, figure 17 shows the spread in reflectivity at the end of the simulation.

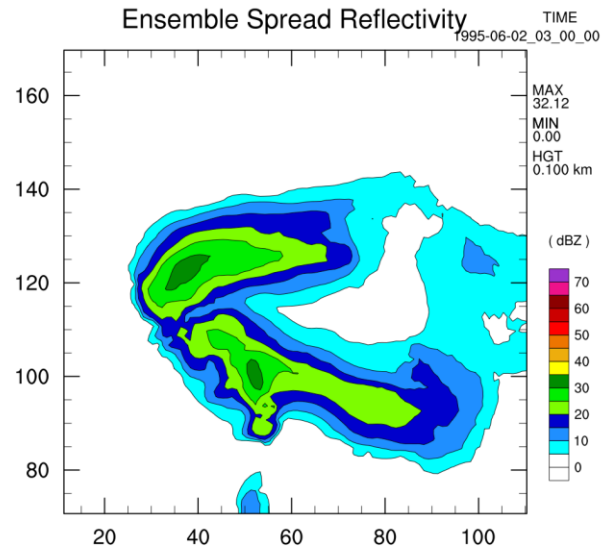


Figure 17: Ensemble spread of radar reflectivity for the CCN ensemble at 3 hours into the model run.

These results demonstrate that uncertainty surrounding a single microphysics parameter can result in significant uncertainty in the forecast, extending as far as to influence the track and intensity of the storm. The notable

variance displayed by all ensembles expresses the need to appropriately represent the range of uncertainty in the microphysics in order to produce a useful forecast.

6. ACKNOWLEDGEMENTS

The first author is supported by the National Science Foundation under Grant No. AGS-1062932 for the Research Experience for Undergraduates through the Center for Analysis and Prediction of Storms.

7. REFERENCES

- Crook, N. A., 1996: Sensitivity of moist convection forced by boundary layer processes to low-level thermodynamic fields. *Mon. Wea. Rev.*, **124**, 1767–1785.
- Dawson, Daniel T., Ming Xue, Jason A. Milbrandt, M. K. Yau, 2010: Comparison of Evaporation and Cold Pool Development between Single-Moment and Multimoment Bulk Microphysics Schemes in Idealized Simulations of Tornadic Thunderstorms. *Mon. Wea. Rev.*, **138**, 1152–1171.
- Ferrier, Brad Schoenberg, 1994: A Double-Moment Multiple-Phase Four-Class Bulk Ice Scheme. Part I: Description. *J. Atmos. Sci.*, **51**, 249–280.
- Ferrier, Brad Schoenberg, Wei-Kuo Tao, Joanne Simpson, 1995: A Double-Moment Multiple-Phase Four-Class Bulk Ice Scheme. Part II: Simulations of Convective Storms in Different Large-Scale Environments and Comparisons with other Bulk Parameterizations. *J. Atmos. Sci.*, **52**, 1001–1033.
- Gilmore, Matthew S., Jerry M. Straka, Erik N. Rasmussen, 2004: Precipitation and Evolution Sensitivity in Simulated Deep Convective Storms: Comparisons between Liquid-Only and Simple Ice and Liquid Phase Microphysics*. *Mon. Wea. Rev.*, **132**, 1897–1916.
- Gilmore, Matthew S., Jerry M. Straka, Erik N. Rasmussen, 2004: Precipitation Uncertainty Due to Variations in Precipitation Particle Parameters within a Simple Microphysics Scheme. *Mon. Wea. Rev.*, **132**, 2610–2627.
- Klemp, Joseph B., Robert B. Wilhelmson, 1978: The Simulation of Three-Dimensional Convective Storm Dynamics. *J. Atmos. Sci.*, **35**, 1070–1096.

- Lin, Yuh-Lang, Richard D. Farley, Harold D. Orville, 1983: Bulk Parameterization of the Snow Field in a Cloud Model. *J. Climate Appl. Meteor.*, **22**, 1065–1092.
- Loftus, Adrian M., Daniel B. Weber, Charles A. Doswell, 2008: Parameterized Mesoscale Forcing Mechanisms for Initiating Numerically Simulated Isolated Multicellular Convection. *Mon. Wea. Rev.*, **136**, 2408–2421.
- Macklin, W. C., 1962: The Density and Structure of Ice Formed by Accretion. *Quart. J. Roy. Meteor. Soc.*, **88**, 30–50.
- Mansell, Edward R., 2010: On Sedimentation and Advection in Multimoment Bulk Microphysics. *J. Atmos. Sci.*, **67**, 3084–3094.
- Mansell, Edward R., Conrad L. Ziegler, Eric C. Bruning, 2010: Simulated Electrification of a Small Thunderstorm with Two-Moment Bulk Microphysics. *J. Atmos. Sci.*, **67**, 171–194.
- Mansell, Edward R., Ziegler, Conrad L., 2010: CCN Effects on Simulated Electrification and Precipitation. *Proc. Conf. Planned and Inadvertent Weather Mod.*, Seattle, WA, Amer. Meteor. Soc., J15.2. [Available online at <http://ams.confex.com/ams/91Annual/webprogram/Manuscript/Paper180497/Mansell.Ziegler.ams2011a.pdf>.]
- Milbrandt, J. A., M. K. Yau, 2005: A Multimoment Bulk Microphysics Parameterization. Part I: Analysis of the Role of the Spectral Shape Parameter. *J. Atmos. Sci.*, **62**, 3051–3064.
- Pflaum, J. C., H. R. Pruppacher, 1979: A Wind Tunnel Investigation of the Growth of Graupel Initiated from Frozen Drops. *J. Atmos. Sci.*, **36**, 680–689.
- Rasmussen, R. M., A. J. Heymsfield, 1985: A Generalized Form for Impact Velocities Used to Determine Graupel Accretional Densities. *J. Atmos. Sci.*, **42**, 2275–2279.
- Stensrud, David J., and Coauthors, 2009: Convective-Scale Warn-on-Forecast System. *Bull. Amer. Meteor. Soc.*, **90**, 1487–1499.
- Stensrud, David J., Jian-Wen Bao, Thomas T. Warner, 2000: Using Initial Condition and Model Physics Perturbations in Short-Range Ensemble Simulations of Mesoscale Convective Systems. *Mon. Wea. Rev.*, **128**, 2077–2107.
- Straka, Jerry M., Edward R. Mansell, 2005: A Bulk Microphysics Parameterization with Multiple Ice Precipitation Categories. *J. Appl. Meteor.*, **44**, 445–466.
- Weisman, M. L., J. B. Klemp, 1982: The Dependence of Numerically Simulated Convective Storms on Vertical Wind Shear and Buoyancy. *Mon. Wea. Rev.*, **110**, 504–520.
- Weisman, Morris L., Joseph B. Klemp, 1984: The Structure and Classification of Numerically Simulated Convective Storms in Directionally Varying Wind Shears. *Mon. Wea. Rev.*, **112**, 2479–2498.
- Wilhelmson, Robert B., Joseph B. Klemp, 1981: A Three-Dimensional Numerical Simulation of Splitting Severe Storms on 3 April 1964. *J. Atmos. Sci.*, **38**, 1581–1600.
- Wisner, Chester, H. D. Orville, Carol Myers, 1972: A Numerical Model of a Hail-Bearing Cloud. *J. Atmos. Sci.*, **29**, 1160–1181.
- Ziegler, Conrad L., 1988: Retrieval of Thermal and Microphysical Variables in Observed Convective Storms. Part II: Sensitivity of Cloud Processes to Variation of the Microphysical Parameterization. *J. Atmos. Sci.*, **45**, 1072–1090.